ACS APPLIED MATERIALS & INTERFACES

Research Article

www.acsami.org

Functionalizing Titanium Disilicide Nanonets with Cobalt Oxide and Palladium for Stable Li Oxygen Battery Operations

Xiahui Yao, Qingmei Cheng, Jin Xie, Qi Dong, and Dunwei Wang*

Department of Chemistry, Merkert Chemistry Center, Boston College, 2609 Beacon St., Chestnut Hill, Massachusetts 02467, United States

Supporting Information

ABSTRACT: Li oxygen ($Li-O_2$) batteries promise high energy densities but suffer from challenges such as poor cycling lifetime and low round-trip efficiencies. Recently, the instability of carbon cathode support has been recognized to contribute significantly to the problems faced by $Li-O_2$ batteries. One strategy to address the challenge is to replace carbon materials with carbon-free ones. Here, we present titanium silicide nanonets ($TiSi_2$) as such a new material platform for this purpose. Because $TiSi_2$ exhibits no oxygen reduction reaction (ORR) or oxygen evolution reaction (OER) activities, catalysts are required to promote discharge and recharge reactions at reduced overpotentials. Pd nanoparticles grown by atomic layer deposition (ALD) were observed to provide the bifunctionalities of ORR and OER. Their adhesion to $TiSi_2$ nanonets, however, was found to be poor, leading to drastic performance decay due to Pd detachments and aggregation. The problem was solved by adding another layer of Co_3O_4, also prepared by ALD. Together, the $Pd/Co_3O_4/TiSi_2$ combination affords the desired functionalities and stability. $Li-O_2$ test cells that lasted more than 126 cycles were achieved. The reversible formation and decomposition of Li_2O_2 was verified by Raman spectroscopy, X-ray photoelectron spectroscopy (XPS), ferrocenium back-titration, and gas-chromatography and mass spectrometry (GC-MS). Our results provide a new material platform for detailed studies of $Li-O_2$ operations for better understanding of the chemistries involved, which is expected to help pave the way toward practical $Li-O_2$ battery realizations.

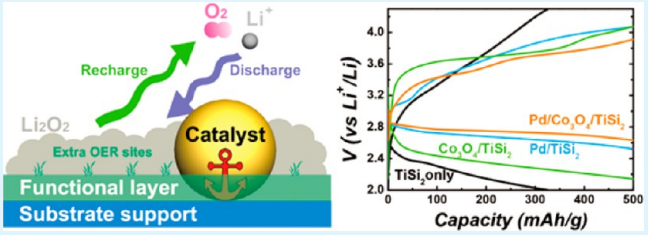

KEYWORDS: *atomic layer deposition, lithium oxygen battery, cathode, catalyst, palladium, cobalt oxide, titanium disilicide*

1. INTRODUCTION

The high theoretical capacities offered by lithium oxygen ($Li-O_2$) batteries hold great promise for meeting our rapidly growing energy storage needs and have motivated significant research efforts.[1] Despite the attention, important challenges remain, including poor cycling performance and low round-trip efficiencies.[2,3] Instabilities of various parts of a $Li-O_2$ test cell, such as the anode, the electrolyte, and the cathode, as well as their synergistic decomposition, are recently recognized as a key issue that needs to be addressed before $Li-O_2$ batteries can be realized as a practical energy storage technology.[4−8] Among the considerations, how carbon-based cathode materials contribute to the parasitic chemistries has attracted increasing research attention.[9] While carbon materials of different forms exhibit good oxygen reduction reaction (ORR) activities in most nonaqueous test electrolytes, which is desired since the ORR activities help reduce discharge overpotentials, carbon has been found to react with reactive intermediates during ORR (e.g., super oxide radicals, $O_2^{\bullet}$).[10] The decomposition of carbon becomes worse during recharge, where high overpotentials are needed to decompose Li_2O_2, especially toward the end of the recharge cycle as carbon does not promote oxygen evolution reactions (OER).[9,11] Indeed, the corrosion of carbon cathode support has been directly observed;[12] isotope experiments have also confirmed that carbon cathode contributes to the deleterious carbonate byproducts formation, manifested as the detection of $^{13}CO_2$ when the cathode was labeled by ^{13}C.[10,13] In principle, the issue may be addressed by concealing active sites on carbon cathode, as has been demonstrated by several recent studies.[14−17] An alternative approach is to seek noncarbon cathode materials, to rid any side-reactions that are directly connected to carbon reactivity.[18−21] Both approaches have their appeals and limitations. For instance, being able to stabilize carbon materials preserves the advantages of low-cost, ease of preparation offered by porous carbon. Noncarbon support, on the other hand, shuts down undesired parasitic chemistries related to carbon reactivity altogether, eliminating potential synergistic effects between electrolyte and carbon decompositions and providing a study platform to understand various processes of $Li-O_2$ operations in great details. Although it remains to be seen which approach (stabilizing or replacing carbon materials) is of greater overall benefits to enable practical $Li-O_2$ batteries, the general consensus is that a noncarbon surface is desired for minimized side reactions on the cathode, where solid Li_2O_2 is formed and decomposed.[13,22,23]

Received: July 20, 2015
Accepted: August 26, 2015
Published: August 26, 2015

DOI: 10.1021/acsami.5b06592
ACS Appl. Mater. Interfaces 2015, 7, 21948−21955

The employment of noncarbon surfaces presents a unique opportunity to study the functions of ORR and OER catalysts. Similar studies on carbon surfaces have yielded seemingly contradictory understandings in the past, and the debates focus on whether the "catalysts" indeed catalyzes Li_2O_2 decomposition or merely alters the interactions between Li_2O_2 and the cathode support.[11,24,25] The ORR activity exhibited by carbon is an important reason for the difference in interpretations. By contrast, except for some rare examples such as porous Au, noncarbon surfaces generally do not exhibit ORR activities.[19,23] This feature allows for understanding the role of catalysts without confounding effects from the cathode support. Here, we demonstrate such a model system based on $TiSi_2$ nanonets, decorated with Pd bifunctional catalysts that promote both ORR and OER. We show that Pd nanoparticles exhibit unambiguous catalytic activity toward ORR and OER in nonaqueous electrolytes. The directly deposited Pd nanoparticles, however, are unstable on $TiSi_2$ surfaces, prone to aggregation and detachment. A functional layer of Co_3O_4 that doubles as an OER catalyst helps immobilize Pd nanoparticles for significantly improved cycling lifetime.

2. EXPERIMENTAL SECTION

2.1. Material Synthesis. $TiSi_2$ nanonets were grown by chemical vapor deposition (CVD). Ti meshes (Cleveland Wire Cloth) were cleaned and used as the substrate. SiH_4 (10% in He, Voltaix), $TiCl_4$ (98%, Sigma-Aldrich), and H_2 (industrial grade, Airgas) were introduced to the tube furnace at 675 °C. The growth lasted typically 30−40 min with the pressure maintained at 5 Torr for desired loading. Pd and Co_3O_4 were deposited in a Savannah S100 (Ultratech) atomic layer deposition (ALD) system. For Pd nanoparticles the growth temperature was 200 °C, with $Pd(hfac)_2$ (palladium(II) hexafluoroacetylacetonate, heated to 60 °C) and formalin (37 wt % in H_2O, contains 10−15% methanol as stabilizer to prevent polymerization, room temperature) as reaction precursors. The purge gas was N_2 with a 20 sccm (standard cubic centimeter per minute) flow rate. A typical growth sequence was Pd−adsorption−purge−formalin−adsorption−purge, and the durations were 1, 15, 20, 1, 15, and 20 s, respectively, with the stop valve mode turned on. For Co_3O_4 growth, the two precursors were Cobaltocene (98%, Strem, 85 °C) and ozone (~120 mg/L, Savannah ozone generator, with 5 psi pressure and 0.2 L per minute flow rate). A typical growth sequence was Co−adsorption−purge−ozone−reaction−purge, and the durations were 0.5, 15, 30, 0.15, 15, and 30 s, respectively, also with the stop valve mode turned on. For the composite structure, cobalt oxide layer was grown on $TiSi_2$ before the Pd deposition to serve as the functional interfacial layer. The mass loading of Co_3O_4 and Pd loading were 0.05−0.1 mg/cm^2 respectively. The loading quantity of each individual sample was measured by the mass gain after ALD growth using a microbalance (Sartorius, CPA2P, ± 1 μg) and confirmed by the inductively coupled plasma optical emission spectrometry (ICP-OES) using an Agilent 5100 ICP-OES Spectrometer.

2.2. Material Characterization. Samples were imaged using a transmission electron microscope (TEM, JEOL 2010F) operating at an acceleration voltage of 200 kV and a field emission scanning electron microscope (FE-SEM, JEOL 6340F) operating at 10 kV. Raman spectra were obtained in a customized airtight sample holder using Horiba XploRA micro Raman system with excitation laser of 532 nm. The surface species and oxidation states were characterized by X-ray photoelectron spectrometry (K-alpha XPS, Thermo Scientific, Al Kα = 1486.7 eV). X-ray diffraction was performed on PANalytical X'Pert with Cu Kα radiation. UV−vis spectra were obtained by USB4000 spectrometer from Ocean Optics.

2.3. Cell Assembly and Electrochemical Characterization. First, 0.1 M $LiClO_4$ in dimethoxyethane (DME) with water level lower than 10 ppm was used as purchased from Novolyte (BASF). $LiClO_4$ (99.99%, battery grade, Sigma-Aldrich) was further baked at 130 °C under vacuum and then dissolved into ionic liquid ($PYR_{14}TFSI$, Solvionic) to give a 1 M solution. Customized Swagelok-type cells were used as the electrochemistry study platform. Cells were assembled in the glovebox (O_2 and H_2O levels < 0.1 ppm) with Li foil as the anode, 2 Celgard 2500 film sheets as the separator, and 0.1 M $LiClO_4$ in DME as the electrolyte. After cell assembly, O_2 (ultrahigh purity, Airgas) was purged into the cell to replace argon, and the cell was isolated from the gas line after reaching 780 Torr. Electrochemical characterizations were carried out on an electrochemical station (Biologic, VMP3).

For commercial Li_2O_2 oxidation test, Li_2O_2 (90%, Sigma-Aldrich) was dispersed in DME by ultrasonication while sealed under argon. The slurry was drop-coated on the $TiSi_2$ cathode with or without Pd loading to achieve the preloaded cathode.

For the cycling test, $Pd/Co_3O_4/TiSi_2$ nanonets cathodes were first assembled in the cell and cycled in oxygen to remove potential ligand remains on the surface of electrode. The treated cathode was washed and transferred to a new cell for the cycling test.

For comparison in quantification of discharge product, carbon black cathode was prepared by dispersing carbon black (Vulcan XC72) and polytetrafluoroethylene (PTFE, 60 wt % dispersion, Sigma-Aldrich) with weight ratio of 95:5 in isopropyl alcohol (10 mg carbon/mL) and then drop coated on Ti mesh with the loading density of 0.2 mg/cm^2. The cathode was further dried in the vacuum oven at 100 °C overnight.

2.4. Quantification of Discharge and Recharge Products. Ferrocenium hexafluorophosphate (97%, Sigma-Aldrich) was dissolved in the DME and filtered to give 3 mM solution. Calibration curves were generated by quantitatively diluting the original solution with pure DME, and a linear relationship between absorption and molar concentration was obtained. For GC-MS tests, the cathode was first discharged in the DME-based electrolyte under pure O_2 to produce Li_2O_2-loaded electrode and transferred to an ionic liquid based cell for test. UHP-grade helium was used to purge the cell for 60 min to remove residual gases, and the helium flow rate was then fixed at 10 sccm controlled by a mass flow controller as the carrier gas. The content of the gas was sampled with a 0.500 mL gas sampling loop every 5 min automatically for GC-MS analysis (Shimadzu QP2010 Ultra, with Carboxen 1010 PLOT column at 50 °C).

3. RESULTS AND DISCUSSION

3.1. Pd Nanoparticles as Bifunctional Catalyst on $TiSi_2$. Our design is schematically shown in Figure 1. The catalyst

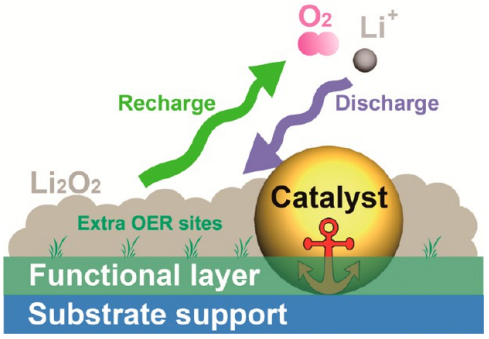

Figure 1. Schematic drawing of the cathode design. The substrate support is $TiSi_2$ nanonets. The functional layer is Co_3O_4. The catalyst is Pd, which promotes both ORR and OER.

used in this study is Pd nanoparticles prepared by atomic layer deposition (ALD). It is anchored on a functional layer of Co_3O_4, the necessity of which will be discussed later. The substrate support is the $TiSi_2$ nanonet, a unique two-dimensional conductive material that has been shown as a good cathode support by us previously when combined with Ru

DOI: 10.1021/acsami.5b06592
ACS Appl. Mater. Interfaces 2015, 7, 21948−21955

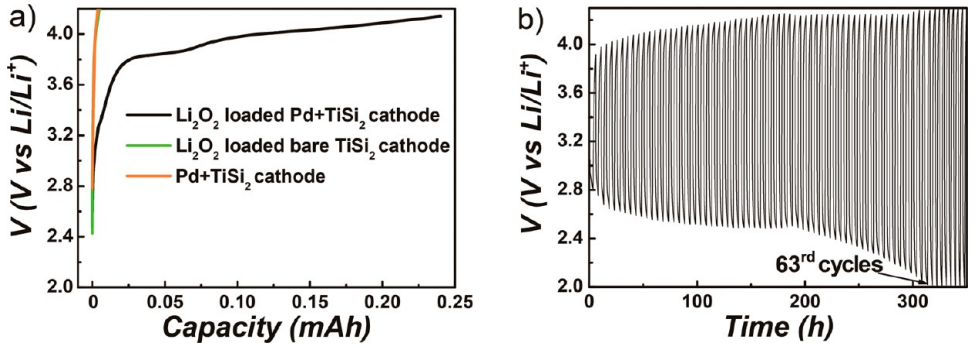

Figure 2. Activities of Pd-decorated $TiSi_2$ nanonets. (a) Direct recharge curves of c-Li_2O_2 mixed $TiSi_2$ nanonets with (black trace) and without (green) Pd nanoparticles. The data from the control sample without c-Li_2O_2 are shown in orange. Current density: 100 mAh/g_{Pd}. (b) Cycling performance of Pd/$TiSi_2$ nanonets. The capacity was limited to 500 mAh/g_{Pd}. Current density: 200 mA/g_{Pd}.

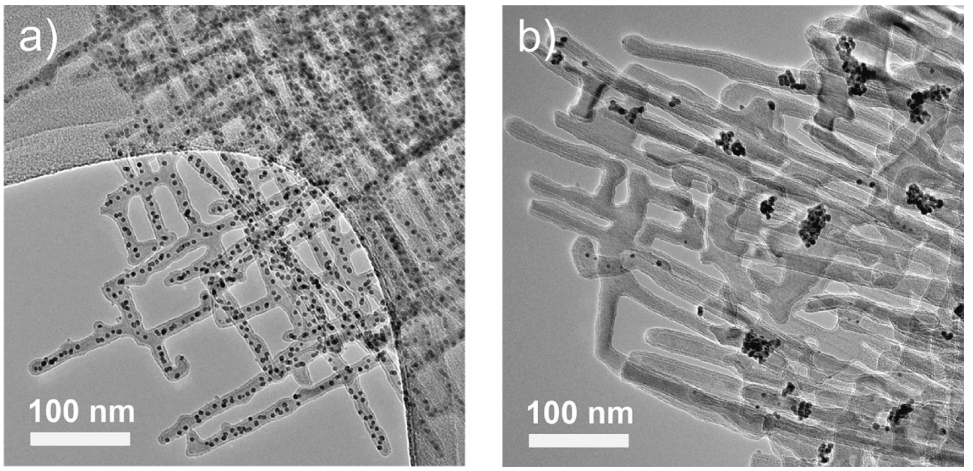

Figure 3. Transmission electron micrographs of Pd/$TiSi_2$ nanonets (a) as-grown and (b) after 63 cycles of discharge/recharge.

nanoparticles.[19,26,27] For the present study, our first task was to investigate whether Pd nanoparticles promote Li_2O_2 decompostion. Although Pd was known as a good ORR catalyst in both aqueous and nonaqueous solutions,[28,29] its activity toward OER has not been conclusively studied on noncarbon substrate.[30] While some reports showed that the addition of Pd to carbon (or noncarbon) cathode reduced the recharge overpotentials,[15,31] the product of Li_2O_2 was found to assume distinct morphologies and crystallinity, upon which the recharge behaviors depend to a great extent.[30,32,33] These varations make it difficult to draw a uniform conclusion about the functionality of Pd. As such, it should be beneficial to confirm whether Pd can promote the decomposition of comercial Li_2O_2, without the variables induced by discharge behaviors.[24] For this purpose, we mixed commerically obtained Li_2O_2 (c-Li_2O_2) with Pd-decorated $TiSi_2$ nanonets (denoted as Pd/$TiSi_2$ henceforth; see Material Synthesis for ALD growth of Pd on $TiSi_2$ nanonets) and measured the voltage of the electrode while maintaining a constant current of 100 mA/g_{Pd} (current normalized to the mass of Pd). It is seen in Figure 2a that the voltage quickly rised from 2.8 V (vs Li/Li^+; all potentials reported in this article are relative to the Li/Li^+ reference electrode) to 3.8 V, a process corresponding to the initial polarization of the electrode for Li_2O_2 decomposition. The rate at which the voltage increases slowed afterward, indicative of steady deomposition of Li_2O_2 above 3.8 V. By contrast, the voltage of the electrode without Pd nanoparticles quickly rised beyond 4.2 V without substantial Li_2O_2 decomposition capacities. To minimize electrolyte decomposition at high potentials, which is common for most electrolyte systems studied to date, we set 4.2 V as the upper limit of the electrode potentials for all electrochemical tests conducted in this article. A third set of data presented in Figure 2a are from the control sample where Pd/$TiSi_2$ was used but without commerical Li_2O_2, and the purpose was to confirm that Pd as a catalyst does not decompose the electrolyte. The results as shown in Figure 2a verify this premise. Taken as a whole, we conclude that Pd nanoparticles grown on $TiSi_2$ nanonets indeed catalyze Li_2O_2 decomposition. Given that the ORR activities of Pd nanoparticles in nonaqueous solutions have been previously demonstrated,[16,31,34] Pd/$TiSi_2$ nanonets should serve as a reasonable cathode electrode to support both Li_2O_2 formation and decomposition. Next, we examined the cycling performance of the electrode in a split test cell with Li foil as the anode and 0.1 M $LiClO_4$ dissolved in dimethoxyethane (DME) as the electrolyte (see Experimental Section). In accordance to the practice commonly adapted in the literature, the cell capacity was limited to 500 mAh/g_{Pd}. It is seen in Figure 2b that the terminal overpotentials for both discharge and recharge, as measured by the difference between the terminal voltages and the thermodynamic equilibrium voltage of $Li_2O_2 \leftrightarrow Li + O_2$ (2.96 V), gradually increased for the first 40 cycles (detailed voltage profiles are shown in Figure S1, Supporting Information). Afterward, the increase became more rapid for the discharge overpotentials, and the discharge

DOI: 10.1021/acsami.5b06592
ACS Appl. Mater. Interfaces 2015, 7, 21948−21955

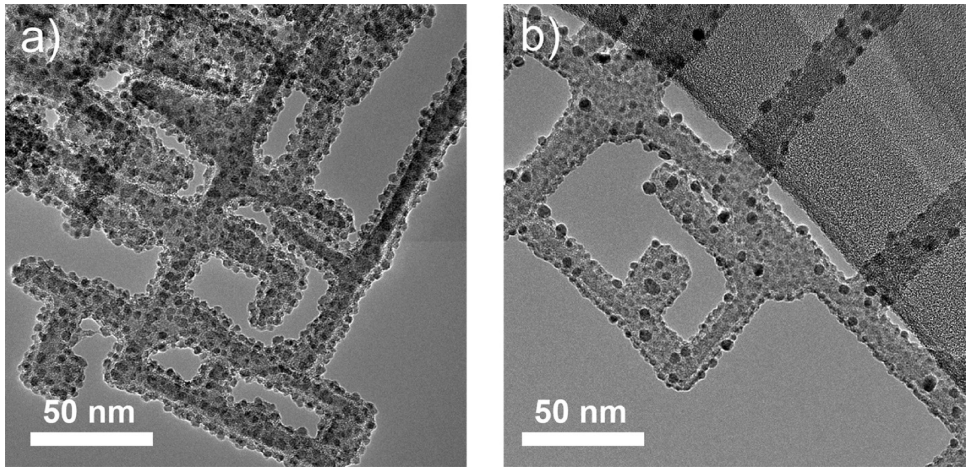

Figure 4. Transmission electron micrographs of functionalized $TiSi_2$ nanonets (a) as-grown Co_3O_4 on $TiSi_2$ nanonet and (b) as-grown $Pd/Co_3O_4/TiSi_2$. Dark particles are Pd, while light contrasted film is Co_3O_4.

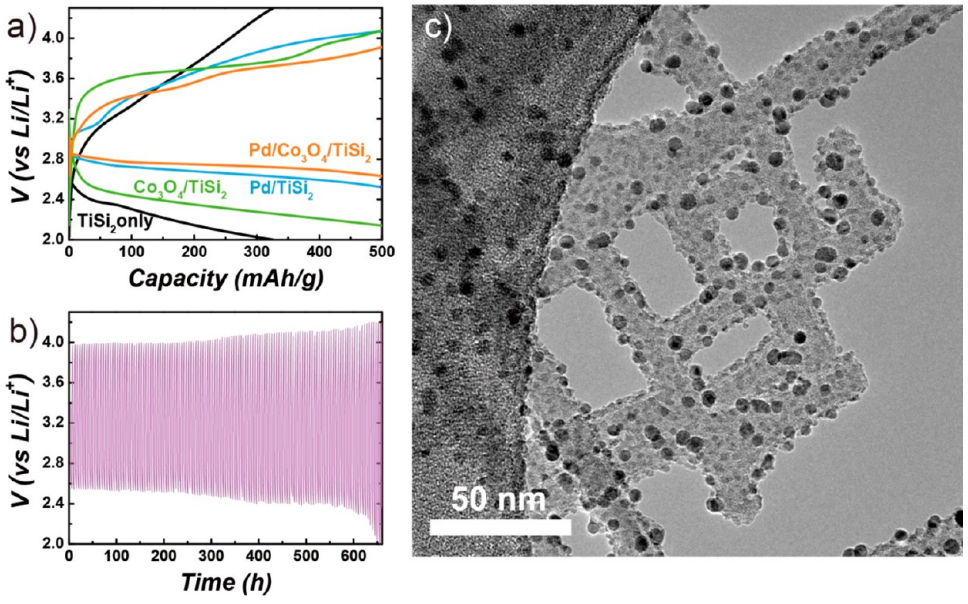

Figure 5. Effects of Co_3O_4 functional layer. (a) Voltage-capacity profiles of $TiSi_2$ (100 mA/g_{TiSi2}), $Co_3O_4/TiSi_2$ (200 mA/g_{Co3O4}), $Pd/TiSi_2$ (200 mA/g_{Pd}), and $Pd/Co_3O_4/TiSi_2$ (200 mA/$g_{Pd+Co3O4}$) cathodes for the first cycle. (b) Voltage−time profile of $Pd/Co_3O_4/TiSi_2$ cathodes for 126 cycles with 500 mAh/$g_{Pd+Co3O4}$ capacity and 200 mA/$g_{Pd+Co3O4}$ current density. (c) TEM image of $Pd/Co_3O_4/TiSi_2$ cathode after 60 cycles still exhibited good dispersion of Pd nanoparticles.

terminal voltage reached 2.0 V at the 63rd cycle, at what point we stopped the experiment.

3.2. Co_3O_4 as Functional Layer for Enhanced Cathode Stability. To understand the degradation mechanism, we examined the $Pd/TiSi_2$ nanonets using transmission electron microscope (TEM). While the distribution of Pd nanoparticles on $TiSi_2$ nanonets right after growth was uniform (Figure 3a), significant detachment and aggregation was observed after repeated discharge and recharge (Figure 3b). The detachment of catalyst particles from their support during electrochemical processes is common.[35,36] For instance, a similar phenomenon has been widely reported for commercial Pt/C catalyst for proton exchange membrane fuel cells.[37,38] It is nevertheless noted that Pt nanoparticles grown on $TiSi_2$ nanonets by ALD were found to be stable upon electrochemical cycling in aqueous electrolytes.[39] Ru nanoparticles grown on $TiSi_2$ nanonets also exhibited remarkable stability when tested under nearly idential conditions to those used in this artile in the same electrolyte ($LiClO_4$ in DME).[19] Our previous studies suggest that the difference in the stabilities may be a result of the difference in the interface energies between $TiSi_2$ and various metal nanoparticles.[19] Among the three, Pd is of the lowest interface energy and is the most prone to detachment (Figure S2, Supporting Information).

The attachment of Pd nanoparticles to $TiSi_2$ nanonets can in principle be strenghtened by the addition of an interfacial layer.[40,41] For this purpose, we chose to deposit Co_3O_4 (Figure 4).[42] We see in Figure 5a that while the presence of Co_3O_4 reduces recharge overpotentials, the presence of Pd is critical to the discharge because neither $TiSi_2$ nor Co_3O_4 surfaces exhibit adequate ORR activities. In other words, as far as single-cycle discharge/recharge is concerned, Pd nanoparticles are sufficient to promote the formation and decomposition of Li_2O_2. Co_3O_4 mainly plays a supporting role in facilitating Li_2O_2 decom-

DOI: 10.1021/acsami.5b06592
ACS Appl. Mater. Interfaces 2015, 7, 21948−21955

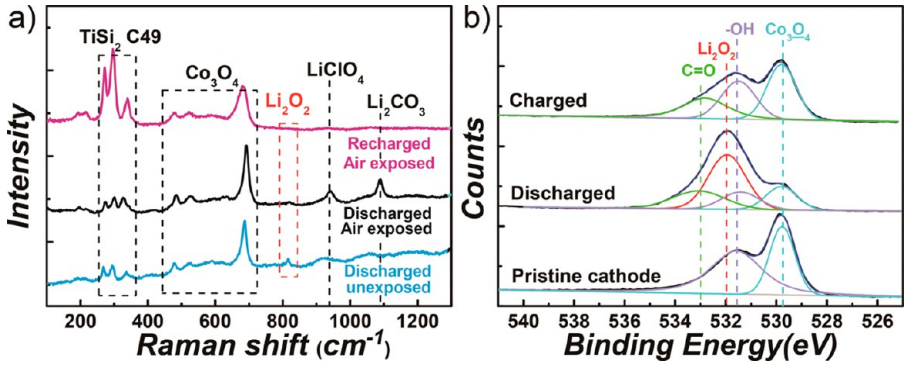

Figure 6. Production detection shown by (a) Raman spectra of discharged and recharged cathode made of $Pd/Co_3O_4/TiSi_2$ and (b) XPS spectra of O 1s binding energies of as-made (pristine), discharged, and recharged cathode surfaces.

position, reducing the recharge overpotential by a marginal 200 mV.[24,43,44] The real benefit of Co_3O_4 became obvious when the cell was tested for extended period of time, lasting 126 cycles (Figure 5b, detailed voltage-capacity profile in Figure S3, Supporting Information), as opposed to 63 cycles without Co_3O_4. As a comparison, typical cells made of carbon-based materials often fail after 10 to 20 cycles of discharge/recharge.[1616] It is noted that while some extraordinary cycling performance (>200 cycles) has been reported, more rigorous detection of Li_2O_2 as the discharge product and O_2 as the recharge product for these reported long cycling cells is often missing to prove the cycling was indeed a result of Li_2O_2 formation and decomposition. More discussions on this point will be presented later in this study. The outstanding stability enabled by the $Pd/Co_3O_4/TiSi_2$ combination is understood as the immobilization effect offered by Co_3O_4, as evidenced by TEM studies on the electrode after 60 cycles of discharge/recharge (Figure 5b), where no obvious changes to the morphology or distribution of Pd nanoparticles are observed.

Because various side reactions, including the electrolyte decomposition, oxidation of the anode, and cathode degradation, can yield artifacts in the electrochemical data that may be mistaken as the purported results,[45] it is of paramount importance to estabilish the measured charges indeed correspond to Li_2O_2 formation and decomposition at or near 100% Faradaic efficiencies. We employed a suite of techniques for this purpose, both qualitative (Raman and XPS, for the confirmation of Li_2O_2 formation) and quantitative (titration and mass-spectrometry, for the quantification of Li_2O_2, as well as O_2 as the decomposition product). The results are presented and discussed next.

3.3. Raman Spectroscopy. After discharge, the test cell was disassembled in an O_2-tolarating Ar glovebox (O_2 concentration <0.1%; H_2O concentration <0.1 ppm with a dew point of −99 °C), and the cathode material was washed with anhydrous DME to remove remaining $LiClO_4$ salt and then sealed in a custom-built container that features a thin glass window, through which the Raman signals were collected. The procedure ensures that the discharged cathode is not exposed to ambient air, to prevent Li_2O_2 from transforming into other compositions (such as LiOH or Li_2CO_3) upon contact with H_2O and CO_2. The detected features are plotted in Figure 6a, where the peaks at ca. 300 cm^{-1} are from $TiSi_2$ (C49 phase), the peaks between 450 to 700 cm^{-1} correspond to Co_3O_4, and the peak at ca. 950 cm^{-1} is from residual $LiClO_4$. Of them, we emphasize the peak at ca. 810 cm^{-1}, which is close to, but does not overlap exactly with, the Raman shift mesaured on commercial Li_2O_2 (790 cm^{-1}). After considering all possible related product (Figure S4, Supporting Information), we concluded that this peak corresponds to Li_2O_2 formed during discharge. Note that direct observations of Li_2O_2 formed during discharge by Raman are not consistent in the literature,[46−48] and many authors, us included, failed to observe the unequivocal evidence of Li_2O_2.[49] We and others have suspected that electrochemically formed Li_2O_2 might differ from commerically obtained crystalline Li_2O_2.[33,50−53] For instance, here, we suggest that the peak shifts (from 790 to 810 cm^{-1}) due to its interactions with the Co_3O_4 surfaces,[43,52] whose Raman shift is also different from that of pristine crystalline Co_3O_4 (Figure S4, Supporting Information). To further support that the peak at 810 cm^{-1} is indeed from Li_2O_2, we next exposed the sample to ambient air. It is expected that the peak at 810 cm^{-1} would decrease and finally diminish, and new peaks corresponding to LiOH and Li_2CO_3 would appear. The observed results indeed confirmed the expectation. As shown in Figure 6a, the peak at 1080 cm^{-1} corresponds to Li_2CO_3; the peaks of LiOH would be buried under those by $TiSi_2$ and were not examined here. Furthermore, no peaks indicative of any of the product (Li_2O_2) or byproduct (Li_2CO_3) are observed on the fully recharged sample.

3.4. X-ray Photoelectron Spectroscopy. By comparing the O 1s spectra of as-made, discharged, and recharged $Pd/Co_3O_4/TiSi_2$ cathode materials, we see a significant evolution of the deconvoluted peak at ~531.9 eV that can be assigned to O in Li_2O_2. The peak was absent after recharge, indicating the successful removal of Li_2O_2. By comparison, the peak at 533.2 eV that can be assigned to O in Li_2CO_3 is only present in the discharged sample due to the exposure of Li_2O_2 to the ambient air (our sample had to be exposed to air briefly during loading into the XPS chamber) and possibly trace amount on the recharged sample from inevitable electrolyte decomposition. Similar result was also observed in the Li 1s spectra (Figure S5, Supporting Information).

3.5. Quantification of Li_2O_2 by Ferrocenium Reduction. As a popularly studied redox pair in a wide range of electrochemical systems, ferrocene/ferrocenium (Fc/Fc^+) is next exploited as a reagent to react with Li_2O_2 for the quantification of the discharge product.[54−56] In essence, we envision that Fc^+ reacts with Li_2O_2 quantitatively following $2Fc^+ + Li_2O_2 \rightarrow Fc + 2Li^+ + O_2$. The changes in the concentration of the Fc^+, tracked by UV−vis spectroscopy through absorption (Figure S6, Supporting Information), can be used to quantify Li_2O_2. The method is similar to the iodometric titrtion that has been applied to quantify Li_2O_2,

DOI: 10.1021/acsami.5b06592
ACS Appl. Mater. Interfaces 2015, 7, 21948−21955

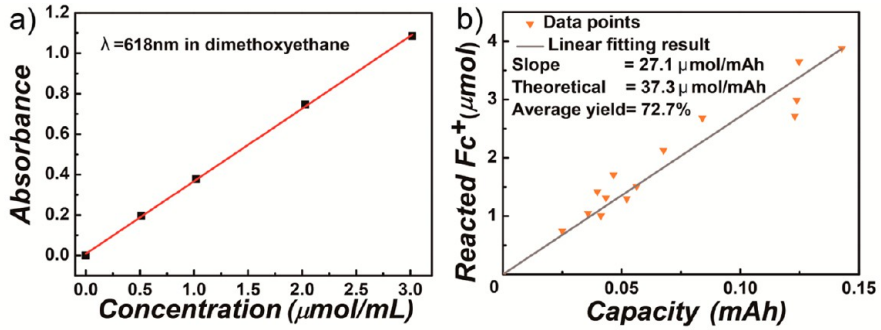

Figure 7. Titration of Li_2O_2 by ferrocenium (Fc^+) reduction. (a) Calibration curve of Fc^+ absorbance at λ = 618 nm. (b) Fc^+ consumption vs discharge capacity plot for quantification of discharge product. For this group of data, an average yield of 72.7% was determined.

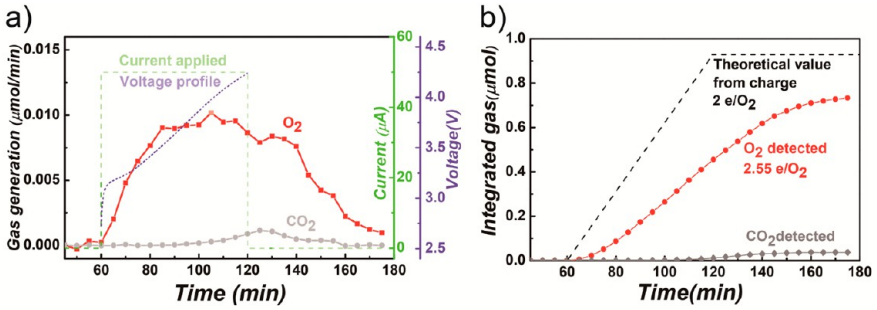

Figure 8. Gas chromatography−mass spectrometry result. (a) Recharge products detected with 50 μA constant current from 60 to 120 min. The corresponding voltage profile (blue dotted line) is superimposed to the graph. (b) The overall gas detected and its comparison to the charge passed.

which is not suitable for our system here due to the catalytic effect of Pd in promoting dispropornation of H_2O_2, an important intermediate in the iodometric titration.[57]

For this set of experiments, a calibration curve that correlates the concentration of Fc^+ and its absorbance at λ = 618 nm was first generated. The good linear relationship (r = 0.99983) provides the basis for the quantification of Li_2O_2 (Figure 7a). The discharged electrode was first removed from the test cell and sealed in a solution (1−2 mL in volume, 3 μmol/g Fc^+) for 20 h to allow for complete reactions. The exact amount of Fc^+ and solvents (DME, which contained phosphorus hexafluoride, PF_6^-, as the counteranion) used for each specific experiment was recorded. The resulting solution was examined again by UV−vis for the end concentration and, hence, the amount of remaining Fc^+. The consumption was deduced from the difference. To eliminate single sample variations and scaling effect, a set of no fewer than 4 tests were performed, and the slope of the Fc^+ consumption rate was used for yield calculation (Figure 7b). When Vulcan carbon was used as a reference, an average total Faradaic efficiency of 74.0% was measured (Figure S7, Supporting Information). Note that the best reported Faradaic efficiencies as quantified by titration method (e.g., iodometric titration; Table S1, Supporting Information) are in the range of 70−83% for Vulcan carbon cathode.[13,22,57] A Faradaic efficiency of 72.7% was obtained on the $Pd/Co_3O_4/TiSi_2$ cathode when the discharge potential was limited to >2.0 V (Figure 7b). The yield was increased to 74.3% when the discharge potential was set at >2.5 V (Figure S8, Supporting Information). It indicates that appreciable side reactions do take place during discharge. More studies are needed to further understand the nature of these side reactions. The extent of the side reactions, however, is not out of line of relevant literature reports.[13,22,57] More importantly, we are confident that all side reactions are entirely due to electrolyte decomposition because the electrodes are carbon-free in our experiments.

3.6. Mass Spectrometry of Recharge Products. The expected gaseous product of Li_2O_2 decomposition is O_2. Under ideal conditions, the amount of O_2 should correspond to the passed charges following a 1:2 ratio (1 O_2 molecule produced by 2 electrons extracted). Gas chromatography−mass spectrometry (GC-MS) is ideal for the detection of O_2 in a quantitative fashion. The technique also allows for the detection of an important byproduct, CO_2. For this purpose, the $Pd/Co_3O_4/TiSi_2$ cathode was first discharged in a DME-based electrolyte. The electrolyte was then replaced by one with significantly reduced vapor pressures, *N*-butyl-*N*-methylpyrrolidinium bis(trifluoromethanesulfonyl) imide ($PYR_{14}TFSI$; 1 M $LiClO_4$ was dissolved for enhanced ionic conductivities; see Methods). The switch of electrolyte was necessary as the high vapor pressure of DME makes it impractical to conduct online detection by GC-MS. Constant current was applied for recharge, and the gaseous products were sampled every 5 min automatically. O_2 (m/z = 32; retention time, 4.9 min) and CO_2 (m/z = 44; retention time, 30 min) counts were recorded (Figure 8a). A rapid rise of O_2 was observed at the beginning of recharge, which tapered off and continued after the recharge was stopped due to the retention of gases by the container. The amount of detected O_2 accounts for 78.4% of the total charges extracted and 93.5% of the total detectable gases (Figure 8b). CO_2 was only observed toward the end of recharge at high applied potentials (>4.0 V), presumably as a result of electrolyte decomposition. No other gaseous product was observed during the whole process. The measured yield is considered relatively high and in line with other reports of 2.45−3.58 e/O_2 during recharge or 74−77% OER/ORR yields.[13,25,57] Factors that contribute to the loss include capacitive behaviors of the electrochemical setup,

DOI: 10.1021/acsami.5b06592
ACS Appl. Mater. Interfaces 2015, 7, 21948−21955

limited yield of Li_2O_2 from discharge, and parasitic reactions of electrolyte decompositions.

4. CONCLUSIONS

In conclusion, we demonstrated that ALD-grown Pd nanoparticles can serve as bifunctional catalysts to enable $TiSi_2$ nanonets as a cathode for Li−O_2 operations. Although successful in promoting both ORR and OER reactions, Pd nanoparticles exhibited severe detachment and aggregation, leading to cell failures after 63 cycles of discharge/recharge. The problem could be addressed by adding a layer of Co_3O_4, also grown by ALD, doubling the cycling lifetime to 126 cycles. The Co_3O_4 not only improved the attachment of Pd nanoparticles, it also helped promote OER for reduced recharge overpotentials. The main discharge products were confirmed as Li_2O_2 by Raman spectroscopy, XPS, and ferrocenium titration. The main recharge products of O_2 were verified by GC-MS. The results further validate $TiSi_2$ as a cathode support for Li−O_2 battery applications. While the design does not solve problems connected to electrolyte decomposition, it helps isolate these issues by eliminating synergistic decompositions between carbon cathode and the electrolyte. The results are expected to contribute to the goal of better understanding, and finally controlling, parasitic chemistries involved in Li−O_2 operation for the realization of the Li−O_2 batteries as a practical energy storage technology.

■ ASSOCIATED CONTENT

Supporting Information

The Supporting Information is available free of charge on the ACS Publications website at DOI: 10.1021/acsami.5b06592.

Full voltage-capacity profile during cycling; additional Raman and XPS results; additional Li_2O_2 quantification results; and SEM images of cathode surfaces. (PDF)

■ AUTHOR INFORMATION

Corresponding Author

* E-mail: dunwei.wang@bc.edu.

Notes

The authors declare no competing financial interest.

■ ACKNOWLEDGMENTS

This work is supported by Boston College. We thank Prof. D. Jiang (UC Riverside) for DFT calculations. We also thank Prof. C.-K. Tsung, Prof. K. R. Metz, Y. Zhang, and I. P. Madden for technical assistance. XPS was performed at the Center for Nanoscale Systems (CNS), a member of the National Nanotechnology Infrastructure Network (NNIN), which is supported by the National Science Foundation under NSF award no. ECS-0335765. CNS is part of Harvard University.

■ REFERENCES

(1) Bruce, P. G.; Freunberger, S. A.; Hardwick, L. J.; Tarascon, J. M. Li-O_2 and Li-S Batteries with High Energy Storage. *Nat. Mater.* **2012**, *11*, 19−29.

(2) Girishkumar, G.; McCloskey, B.; Luntz, A. C.; Swanson, S.; Wilcke, W. Lithium-Air Battery: Promise and Challenges. *J. Phys. Chem. Lett.* **2010**, *1*, 2193−2203.

(3) Lu, Y. C.; Gallant, B. M.; Kwabi, D. G.; Harding, J. R.; Mitchell, R. R.; Whittingham, M. S.; Shao-Horn, Y. Lithium-Oxygen Batteries: Bridging Bechanistic Understanding and Battery Performance. *Energy Environ. Sci.* **2013**, *6*, 750−768.

(4) Xu, W.; Wang, J.; Ding, F.; Chen, X.; Nasybulin, E.; Zhang, Y.; Zhang, J.-G. Lithium Metal Anodes for Rechargeable Batteries. *Energy Environ. Sci.* **2014**, *7*, 513−537.

(5) Li, F.; Zhang, T.; Zhou, H. Challenges of Non-aqueous Li-O_2 Batteries: Electrolytes, Catalysts, and Anodes. *Energy Environ. Sci.* **2013**, *6*, 1125−1141.

(6) Freunberger, S. A.; Chen, Y.; Drewett, N. E.; Hardwick, L. J.; Bardé, F.; Bruce, P. G. The Lithium-Oxygen Battery with Ether-Based Electrolytes. *Angew. Chem., Int. Ed.* **2011**, *50*, 8609−8613.

(7) Kwabi, D. G.; Batcho, T. P.; Amanchukwu, C. V.; Ortiz-Vitoriano, N.; Hammond, P.; Thompson, C. V.; Shao-Horn, Y. Chemical Instability of Dimethyl Sulfoxide in Lithium-Air Batteries. *J. Phys. Chem. Lett.* **2014**, *5*, 2850−2856.

(8) Gittleson, F. S.; Sekol, R. C.; Doubek, G.; Linardi, M.; Taylor, A. D. Catalyst and Electrolyte Synergy in Li-O_2 Batteries. *Phys. Chem. Chem. Phys.* **2014**, *16*, 3230−3237.

(9) Thotiyl, M. M. O.; Freunberger, S. A.; Peng, Z. Q.; Bruce, P. G. The Carbon Electrode in Nonaqueous Li-O_2 Cells. *J. Am. Chem. Soc.* **2013**, *135*, 494−500.

(10) McCloskey, B. D.; Speidel, A.; Scheffler, R.; Miller, D. C.; Viswanathan, V.; Hummelshøj, J. S.; Nørskov, J. K.; Luntz, A. C. Twin Problems of Interfacial Carbonate Formation in Nonaqueous Li-O_2 Batteries. *J. Phys. Chem. Lett.* **2012**, *3*, 997−1001.

(11) Harding, J. R.; Lu, Y. C.; Tsukada, Y.; Shao-Horn, Y. Evidence of Catalyzed Oxidation of Li_2O_2 for Rechargeable Li-Air Battery Applications. *Phys. Chem. Chem. Phys.* **2012**, *14*, 10540−10546.

(12) Itkis, D. M.; Semenenko, D. A.; Kataev, E. Y.; Belova, A. I.; Neudachina, V. S.; Sirotina, A. P.; Hävecker, M.; Teschner, D.; Knop-Gericke, A.; Dudin, P.; Barinov, A.; Goodilin, E. A.; Shao-Horn, Y.; Yashina, L. V. Reactivity of Carbon in Lithium-oxygen Battery Positive Electrodes. *Nano Lett.* **2013**, *13*, 4697−4701.

(13) Adams, B. D.; Black, R.; Radtke, C.; Williams, Z.; Mehdi, B. L.; Browning, N. D.; Nazar, L. F. The Importance of Nanometric Passivating Films on Cathodes for Li-Air Batteries. *ACS Nano* **2014**, *8*, 12483−12493.

(14) Kang, S. J.; Mori, T.; Narizuka, S.; Wilcke, W.; Kim, H.-C. Deactivation of Carbon Electrode for Elimination of Carbon Dioxide Evolution from Rechargeable Lithium-oxygen Cells. *Nat. Commun.* **2014**, *5*, 3937.

(15) Lu, J.; Lei, Y.; Lau, K. C.; Luo, X. Y.; Du, P.; Wen, J. G.; Assary, R. S.; Das, U.; Miller, D. J.; Elam, J. W.; Albishri, H. M.; El-Hady, D. A.; Sun, Y. K.; Curtiss, L. A.; Amine, K. A Nanostructured Cathode Architecture for Low Charge Overpotential in Lithium-Oxygen Batteries. *Nat. Commun.* **2013**, *4*, 2383.

(16) Xie, J.; Yao, X.; Cheng, Q.; Madden, I. P.; Dornath, P.; Chang, C.-C.; Fan, W.; Wang, D. Three Dimensionally Ordered Mesoporous Carbon as a Stable, High-Performance Li-O_2 Battery Cathode. *Angew. Chem., Int. Ed.* **2015**, *54*, 4299−4303.

(17) Jian, Z.; Liu, P.; Li, F.; He, P.; Guo, X.; Chen, M.; Zhou, H. Core-shell-structured CNT@RuO_2 Composite as a High-performance Cathode Catalyst for Rechargeable Li-O_2 Batteries. *Angew. Chem., Int. Ed.* **2014**, *53*, 442−446.

(18) Peng, Z.; Freunberger, S. A.; Chen, Y.; Bruce, P. G. A Reversible and Higher-rate Li-O_2 Battery. *Science* **2012**, *337*, 563−566.

(19) Xie, J.; Yao, X.; Madden, I. P.; Jiang, D.-E.; Chou, L.-Y.; Tsung, C.-K.; Wang, D. Selective Deposition of Ru Nanoparticles on $TiSi_2$ Nanonet and Its Utilization for Li_2O_2 Formation and Decomposition. *J. Am. Chem. Soc.* **2014**, *136*, 8903−8906.

(20) Li, F.; Tang, D.-M.; Chen, Y.; Golberg, D.; Kitaura, H.; Zhang, T.; Yamada, A.; Zhou, H. Ru/ITO: A Carbon-Free Cathode for Nonaqueous Li-O_2 Battery. *Nano Lett.* **2013**, *13*, 4702−4707.

(21) Riaz, A.; Jung, K. N.; Chang, W.; Lee, S. B.; Lim, T. H.; Park, S. J.; Song, R. H.; Yoon, S.; Shin, K. H.; Lee, J. W. Carbon-free Cobalt Oxide Cathodes with Tunable Nanoarchitectures for Rechargeable Lithium-Oxygen Batteries. *Chem. Commun.* **2013**, *49*, 5984−5986.

(22) Nasybulin, E. N.; Xu, W.; Mehdi, B. L.; Thomsen, E.; Engelhard, M. H.; Massé, R. C.; Bhattacharya, P.; Gu, M.; Bennett, W.; Nie, Z.; Wang, C.; Browning, N. D.; Zhang, J.-G. Formation of Interfacial

DOI: 10.1021/acsami.5b06592
ACS Appl. Mater. Interfaces 2015, 7, 21948−21955

Layer and Long-Term Cyclability of Li-O_2 Batteries. *ACS Appl. Mater. Interfaces* **2014**, *6*, 14141−14151.
(23) Ottakam Thotiyl, M. M.; Freunberger, S. A.; Peng, Z.; Chen, Y.; Liu, Z.; Bruce, P. G. A Stable Cathode for the Aprotic Li-O_2 Battery. *Nat. Mater.* **2013**, *12*, 1050−1056.
(24) Black, R.; Lee, J.-H.; Adams, B.; Mims, C. A.; Nazar, L. F. The Role of Catalysts and Peroxide Oxidation in Lithium-Oxygen Batteries. *Angew. Chem., Int. Ed.* **2013**, *52*, 392−396.
(25) McCloskey, B. D.; Bethune, D. S.; Shelby, R. M.; Mori, T.; Scheffler, R.; Speidel, A.; Sherwood, M.; Luntz, A. C. Limitations in Rechargeability of Li-O_2 Batteries and Possible Origins. *J. Phys. Chem. Lett.* **2012**, *3*, 3043−3047.
(26) Zhou, S.; Liu, X.; Lin, Y.; Wang, D. Spontaneous Growth of Highly Conductive Two-Dimensional Single-Crystalline $TiSi_2$ Nanonets. *Angew. Chem., Int. Ed.* **2008**, *47*, 7681−7684.
(27) Zhou, S.; Yang, X.; Xie, J.; Simpson, Z. I.; Wang, D. Titanium Silicide Nanonet as a New Material Platform for Advanced Lithium Ion Battery Applications. *Chem. Commun.* **2013**, *49*, 6470−6476.
(28) Cui, Z.; Li, L.; Manthiram, A.; Goodenough, J. B. Enhanced Cycling Stability of Hybrid Li-Air Batteries Enabled by Ordered Pd_3Fe Intermetallic Electrocatalyst. *J. Am. Chem. Soc.* **2015**, *137*, 7278−7281.
(29) Wang, Z.-L.; Xu, D.; Xu, J.-J.; Zhang, X.-B. Oxygen Electrocatalysts in Metal-Air Batteries: from Aqueous to Nonaqueous Electrolytes. *Chem. Soc. Rev.* **2014**, *43*, 7746−7786.
(30) Xu, J.-J.; Wang, Z.-L.; Xu, D.; Zhang, L.-L.; Zhang, X.-B. Tailoring Deposition and Morphology of Discharge Products Towards High-rate and Long-life Lithium-oxygen Batteries. *Nat. Commun.* **2013**, *4*, 2438.
(31) Lei, Y.; Lu, J.; Luo, X.; Wu, T.; Du, P.; Zhang, X.; Ren, Y.; Wen, J.; Miller, D. J.; Miller, J. T.; Sun, Y.-K.; Elam, J. W.; Amine, K. Synthesis of Porous Carbon Supported Palladium Nanoparticle Catalysts by Atomic Layer Deposition: Application for Rechargeable Lithium-O_2 Battery. *Nano Lett.* **2013**, *13*, 4182−4189.
(32) Gallant, B. M.; Kwabi, D. G.; Mitchell, R. R.; Zhou, J.; Thompson, C. V.; Shao-Horn, Y. Influence of Li_2O_2 Morphology on Oxygen Reduction and Evolution Kinetics in Li-O_2 Batteries. *Energy Environ. Sci.* **2013**, *6*, 2518−2528.
(33) Yilmaz, E.; Yogi, C.; Yamanaka, K.; Ohta, T.; Byon, H. R. Promoting Formation of Noncrystalline Li_2O_2 in the Li-O_2 Battery With RuO_2 Nanoparticles. *Nano Lett.* **2013**, *13*, 4679−4684.
(34) Lu, Y.-C.; Gasteiger, H. A.; Shao-Horn, Y. Catalytic Activity Trends of Oxygen Reduction Reaction for Nonaqueous Li-Air Batteries. *J. Am. Chem. Soc.* **2011**, *133*, 19048−19051.
(35) Ferreira, P. J.; la O', G. J.; Shao-Horn, Y.; Morgan, D.; Makharia, R.; Kocha, S.; Gasteiger, H. A. Instability of Pt/C Electrocatalysts in Proton Exchange Membrane Fuel Cells: A Mechanistic Investigation. *J. Electrochem. Soc.* **2005**, *152*, A2256−A2271.
(36) Morales-Guio, C. G.; Tilley, S. D.; Vrubel, H.; Gratzel, M.; Hu, X. Hydrogen Evolution From a Copper(I) Oxide Photocathode Coated with An Amorphous Molybdenum Sulphide Catalyst. *Nat. Commun.* **2014**, *5*, 3059.
(37) Shao, Y.; Yin, G.; Gao, Y. Understanding and Approaches for the Durability Issues of Pt-based Catalysts for PEM Fuel Cell. *J. Power Sources* **2007**, *171*, 558−566.
(38) Yu, X.; Ye, S. Recent Advances in Activity and Durability Enhancement of Pt/C Catalytic Cathode in PEMFC: Part II: Degradation Mechanism and Durability Enhancement of Carbon Supported Platinum Catalyst. *J. Power Sources* **2007**, *172*, 145−154.
(39) Xie, J.; Yang, X. G.; Han, B. H.; Shao-Horn, Y.; Wang, D. W. Site-Selective Deposition of Twinned Platinum Nanoparticles on $TiSi_2$ Nanonets by Atomic Layer Deposition and Their Oxygen Reduction Activities. *ACS Nano* **2013**, *7*, 6337−6345.
(40) Elam, J. W.; Zinovev, A.; Han, C. Y.; Wang, H. H.; Welp, U.; Hryn, J. N.; Pellin, M. J. Atomic Layer Deposition of Palladium Films on Al_2O_3 Surfaces. *Thin Solid Films* **2006**, *515*, 1664−1673.
(41) Han, X.; Liu, Y.; Jia, Z.; Chen, Y.-C.; Wan, J.; Weadock, N.; Gaskell, K. J.; Li, T.; Hu, L. Atomic-Layer-Deposition Oxide Nanoglue for Sodium Ion Batteries. *Nano Lett.* **2014**, *14*, 139−147.
(42) Diskus, M.; Nilsen, O.; Fjellvåg, H. Thin Films of Cobalt Oxide Deposited on High Aspect Ratio Supports by Atomic Layer Deposition. *Chem. Vap. Deposition* **2011**, *17*, 135−140.
(43) Su, D.; Dou, S.; Wang, G. Single Crystalline Co_3O_4 Nanocrystals Exposed with Different Crystal Planes for Li-O_2 Batteries. *Sci. Rep.* **2014**, *4*, 5767.
(44) Ryu, W.-H.; Yoon, T.-H.; Song, S. H.; Jeon, S.; Park, Y.-J.; Kim, I.-D. Bifunctional Composite Catalysts Using Co_3O_4 Nanofibers Immobilized on Nonoxidized Graphene Nanoflakes for High-Capacity and Long-Cycle Li-O_2 Batteries. *Nano Lett.* **2013**, *13*, 4190−4197.
(45) McCloskey, B. D.; Bethune, D. S.; Shelby, R. M.; Girishkumar, G.; Luntz, A. C. Solvents' Critical Role in Nonaqueous Lithium-Oxygen Battery Electrochemistry. *J. Phys. Chem. Lett.* **2011**, *2*, 1161−1166.
(46) Thapa, A. K.; Shin, T. H.; Ida, S.; Sumanasekera, G. U.; Sunkara, M. K.; Ishihara, T. Gold-palladium Nanoparticles Supported by Mesoporous β-MnO_2 Air Electrode for Rechargeable Li-Air Battery. *J. Power Sources* **2012**, *220*, 211−216.
(47) Peng, Z.; Freunberger, S. A.; Hardwick, L. J.; Chen, Y.; Giordani, V.; Bardé, F.; Novák, P.; Graham, D.; Tarascon, J.-M.; Bruce, P. G. Oxygen Reactions in a Non-Aqueous Li^+ Electrolyte. *Angew. Chem., Int. Ed.* **2011**, *50*, 6351−6355.
(48) Zhai, D.; Wang, H.-H.; Lau, K. C.; Gao, J.; Redfern, P. C.; Kang, F.; Li, B.; Indacochea, E.; Das, U.; Sun, H.-H.; Sun, H.-J.; Amine, K.; Curtiss, L. A. Raman Evidence for Late Stage Disproportionation in a Li-O_2 Battery. *J. Phys. Chem. Lett.* **2014**, *5*, 2705−2710.
(49) Xu, C.; Gallant, B. M.; Wunderlich, P. U.; Lohmann, T.; Greer, J. R. Three-Dimensional Au Microlattices as Positive Electrodes for Li-O_2 Batteries. *ACS Nano* **2015**, *9*, 5876−5883.
(50) Yang, J.; Zhai, D.; Wang, H.-H.; Lau, K. C.; Schlueter, J. A.; Du, P.; Myers, D. J.; Sun, Y.-K.; Curtiss, L. A.; Amine, K. Evidence for Lithium Superoxide-like Species in the Discharge Product of a Li-O_2 Battery. *Phys. Chem. Chem. Phys.* **2013**, *15*, 3764−3771.
(51) Zhu, J.; Ren, X.; Liu, J.; Zhang, W.; Wen, Z. Unraveling the Catalytic Mechanism of Co_3O_4 for the Oxygen Evolution Reaction in a Li-O_2 Battery. *ACS Catal.* **2015**, *5*, 73−81.
(52) Radin, M. D.; Monroe, C. W.; Siegel, D. J. How Dopants Can Enhance Charge Transport in Li_2O_2. *Chem. Mater.* **2015**, *27*, 839−847.
(53) Eysel, H. H.; Thym, S. RAMAN Spectra of Peroxides. *Z. Anorg. Allg. Chem.* **1975**, *411*, 97−102.
(54) Ding, Y.; Zhao, Y.; Yu, G. A Membrane-Free Ferrocene-Based High-Rate Semiliquid Battery. *Nano Lett.* **2015**, *15*, 4108−4113.
(55) Chen, Y.; Freunberger, S. A.; Peng, Z.; Fontaine, O.; Bruce, P. G. Charging a Li-O_2 Battery Using a Redox Mediator. *Nat. Chem.* **2013**, *5*, 489−494.
(56) Hase, Y.; Ito, E.; Shiga, T.; Mizuno, F.; Nishikoori, H.; Iba, H.; Takechi, K. Quantitation of Li_2O_2 stored in Li-O_2 Batteries Based on Its Reaction with an Oxoammonium Salt. *Chem. Commun.* **2013**, *49*, 8389−8391.
(57) McCloskey, B. D.; Valery, A.; Luntz, A. C.; Gowda, S. R.; Wallraff, G. M.; Garcia, J. M.; Mori, T.; Krupp, L. E. Combining Accurate O_2 and Li_2O_2 Assays to Separate Discharge and Charge Stability Limitations in Nonaqueous Li-O_2 Batteries. *J. Phys. Chem. Lett.* **2013**, *4*, 2989−2993.

DOI: 10.1021/acsami.5b06592
ACS Appl. Mater. Interfaces 2015, 7, 21948−21955